Mass Transport through Carbon Nanotube Membranes in Three Different Regimes: Ionic Diffusion and Gas and Liquid Flow

Mainak Majumder,[†,⊥] Nitin Chopra,[‡,∥] and Bruce J. Hinds[†,‡,*]

[†]Department of Chemical & Materials Engineering, University of Kentucky, Lexington, Kentucky 40506-0046, United States, and [‡]Department of Chemistry, University of Kentucky, Lexington, Kentucky 40506-0046, United States. [⊥] Present address: Nanoscale Science and Engineering Laboratory (NSEL), Monash University, Australia. [∥] Present address: Metallurgical and Materials Engineering Center for Materials for Information Technology (MINT), University of Alabama, Tuscaloosa, AL 35487.

ABSTRACT Transport phenomena through the hollow conduits of carbon nanotubes (CNTs) are subjects of intense theoretical and experimental research. We have studied molecular transport over the large spectrum of ionic diffusion to pressure-driven gaseous and liquid flow. Plasma oxidation during the fabrication of the membrane introduces carboxylic acid groups at the CNT entrance, which provides electrostatic "gatekeeper" effects on ionic transport. Diffusive transport of ions of different charge and size through the core of the CNT is close to bulk diffusion expectations and allows estimation of the number of open pores or porosity of the membrane. Flux of gases such as N_2, CO_2, Ar, H_2, and CH_4 scaled inversely with their molecular weight by an exponent of 0.4, close to expected kinetic theory velocity expectations. However, the magnitude of the fluxes was ~15- to 30-fold higher than predicted from Knudsen diffusion kinetics and consistent with specular momentum reflection inside smooth pores. Polar liquids such as water, ethanol, and isopropyl alcohol and nonpolar liquids such as hexane and decane were dramatically enhanced, with water flow over 4 orders of magnitude larger than "no-slip" hydrodynamic flow predictions. As direct experimental proof for the mechanism of near perfect slip conditions within CNT cores, a stepwise hydrophilic functionalization of CNT membranes from as-produced, tip-functionalized, and core-functionalized was performed. Pressure-driven water flow through the membrane was reduced from 5×10^4 to 2×10^2 to less than a factor of 5 enhancement over conventional Newtonian flow, while retaining nearly the same pore area.

KEYWORDS: membrane · separations · biomimetic · nanofluidics

Biological protein channels are remarkable systems that have the ability to selectively pump necessary chemicals and signals through cell walls at rates that are orders of magnitude faster than inorganic pores with near perfect selection. Mimicking this function in large-area robust man-made structures can have broad applications in water purification, chemical separations, drug delivery, and sensing. The key to Nature's channels are (1) selective receptor chemistry at the pore entrance, (2) a mechanism for fast fluid flow or mass-transport, and (3) a signal at the exit side of the protein to activate the channel.[1] Pioneering efforts toward this goal have focused on well-ordered nanoporous monoliths such as porous alumina or track-etched polycarbonate with minimal path tortuosity, ability to reduce pore size to the nanometer scale, and ability to add selective surface chemistry.[2−6] However these approaches suffer from the common problems of an inability to place an effective monolayer of gatekeeper chemistry at the pore entrance and the inherently slow process of fluid flow in nanometer-scale pores. In particular, pressure-driven fluid flow in nanometer-scale pores is acutely limited by the boundary condition of zero flow velocity on the pore wall and can thus reach only minute core velocities through the sheer of Newtonian fluids. Natural protein channels are able to support very fast interfacial velocities in the pores, as is seen with the single file flow of highly oriented waters through the aquapourin channel.

The inner cores of carbon nanotubes (CNTs) have the potential to exhibit a fast interfacial "slip velocity" at the pore wall due to CNTs having a large noninteracting van der Waals distance and an atomically flat surface that would not scatter flowing fluids. An early molecular dynamics simulation study[7] predicts strong self-associating H-bond coupling of water within a "hydrophobic" single-walled CNTs (SWCNTs) and 5 orders of magnitude faster flow than would be expected for conventional materials. This flow rate is similar to what is seen in the aquapourin protein channel that pumps water across kidney membranes. High flow velocities of molecules were also predicted simply based on the near frictionless nature of the CNT walls[8,9] as well as the fast diffusion rates for hydrocarbons.[10−12] In the

* Address correspondence to bjhinds@engr.uky.edu.

Received for review January 19, 2011 and accepted April 18, 2011.

Published online April 18, 2011
10.1021/nn200222g

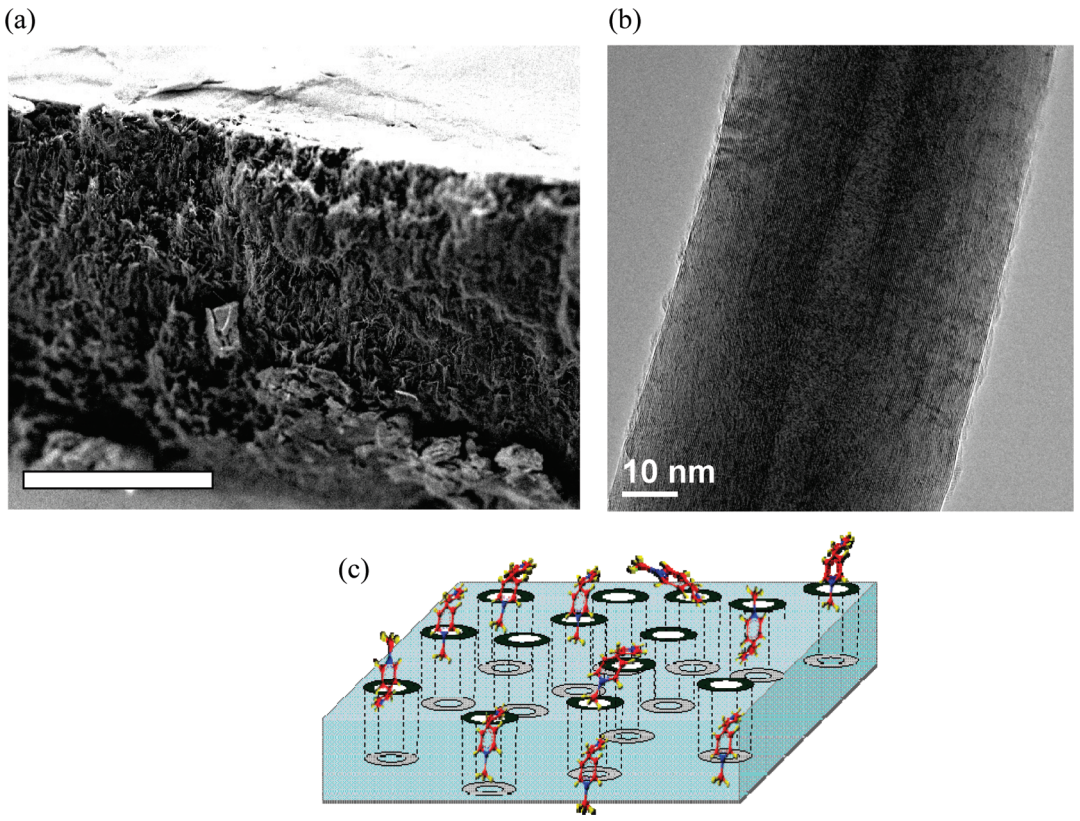

Figure 1. (a) Scanning electron micrograph of the CNT membrane used in the study; scale bar is 10 μm. (b) HR-TEM image of MWCNT showing ~7 nm i.d. inner core. (c) Schematic of the theme of the present study: molecular transport through the inner core of the CNTs to pass across the membrane structure.

latter case, favorable interactions of the methane with the CNT wall predict the molecule will "skate" down the tube wall and not scatter in random directions, as would conventionally happen in the case of Knudsen diffusion. The flow velocity of gaseous methane is predicted to be ~260 cm/s at 1 bar.[10] In all models, the atomically flat nature of graphite sheets inherent to the CNT microstructure makes the enhanced flow possible over long length scales. In fact, if a radial atomic step edge is placed inside a CNT core, there is a dramatic drop in predicted flow rates due to interfacial scattering.[13] Recently a new class of membranes with highly ordered graphitic CNTs as conduits[14−19] have demonstrated extremely fast transport.[15,20] The process entails encapsulation of vertically oriented CNT mats inside an inert polymer[14] or a ceramic matrix[15] with a plasma etching-based chemistry opening up the CNT tips.

The present study experimentally investigates mass transport through the aligned multiwalled CNT membrane structure with ~7 nm pore diameter, in the broad spectrum of ionic diffusion and pressure-driven liquid and gas transport. The membrane structure of interest contains a substantially large number of CNTs (~10^{10}/cm^2), which allows macroscopic measurement of transport through the membrane. Experimental transport properties are compared with conventional models of mass transport through membranes of comparable pore size and show that nanoscale transport phenomena in these graphitic pores are dramatically enhanced.

RESULTS AND DISCUSSIONS

Ionic Transport and Gatekeeper Activity. To mimic protein channels, it is necessary to have selective chemistry at the channel entrance to act as a gatekeeper or chemically activated pump as diagrammed in Figure 1. An integral part of the membrane fabrication procedure is the plasma-oxidation process that opens the previously sealed CNTs, potentially allowing functional chemistry at only the tip region. Experimental results indicate that liquid phase treatments tend to introduce carboxylic acid groups, whereas gas phase treatments introduce less oxidized groups such as hydroxy and carbonyl.[21,22] Therefore, water vapor plasma treatment for opening the CNTs is most likely to introduce carboxyl groups on the tips of the CNT membrane. Because the high-energy plasma would react with the initial contact surface, this precludes its entrance deep into the pores, limiting the functionalization to the surface and near tip regions.[23] The surface density of carboxyl groups can be increased significantly by utilizing a one-electron reduction of diazonium salts containing a terminal carboxylic acid group.[24] The

TABLE 1. Molecules with Varying Size and Charge Density to Study Diffusion through Carbon Nanotube Membranes[a]

Probe	Structure	Bulk Diffusivity (cm^2/s)	Stoke-Einstein Diameter (A^0)	Apparent Diffusivity (cm^2/s)
Methyl Violgen (MV^{2+})	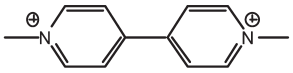	7.74×10^{-6}	6.3	7.92×10^{-6}
Ruthenium bi-pyridine ($Ru(bipy)_3^{2+}$)	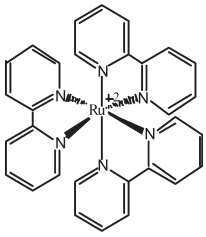	5.16×10^{-6}	9.5	4.78×10^{-6}
2,6 naphthalene di-sulfonic acid (NDS^{2-})	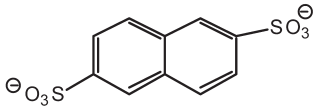	5.77×10^{-6}	8.5	4.26×10^{-6}
Fast Green (Green Dye^{2-})	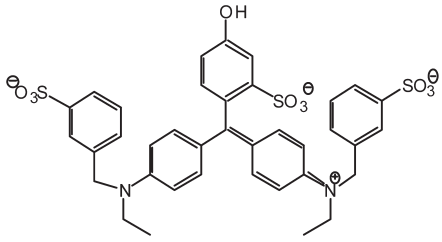	2.90×10^{-6}	16.9	1.10×10^{-6}
Rhodamine B (Rhod)	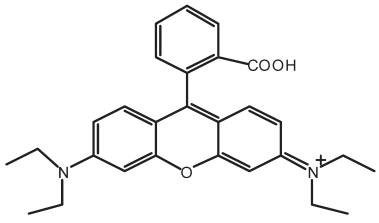	3.60×10^{-6}	13.62	1.98×10^{-6}

[a] Shown is their bulk diffusivity and experimentally observed diffusivity through the as-made CNT membrane.

deprotonated carboxylic groups on the membrane surface lead to an increase of interfacial capacitance with increasing pH. Qualitatively, one can estimate a ~2−2.5-fold increase in functional density after diazonium grafting chemistry;[25] however, a small increase of capacitance of the as-made CNT membrane indicates the presence of surface carboxyl groups from the plasma-oxidation.

Ionic transport of similarly charged but differently sized probes through CNT membrane could be modulated by chemical gatekeeper functionality at CNT entrances.[26] The factors affecting transport were chain length, solubility/conformation, charge of the functional molecule, and solution ionic strength. Of interest in this study is to understand ionic transport of a variety of ions of different size and charge through the inner core of CNTs. The structure, bulk diffusivity, and apparent diffusivity of the probe molecules are shown in Table 1. The bulk diffusivity values are from literature precedence[27−29] for MV^{2+}, $Ru(bipy)_3^{2+}$, NDS^{2-}, and Rhod, whereas the bulk diffusivity of green dye^{2-} has been calculated from Wilkie−Chang correlation. The Stokes−Einstein diameter of these probe molecules has been calculated from the relation

$$D_0 = \frac{kT}{6\pi\eta R_s} \quad (1)$$

where D_0 is the bulk diffusivity, k is the Boltzmann constant, η is the viscosity of the liquid, and R_s is the spherical radius of the molecule. The Stokes−Einstein diameter calculated from the aforementioned equation provides a value for the hydrodynamic size of the diffusing species and is very pertinent to the diffusion analysis in this study. The apparent diffusivity of the

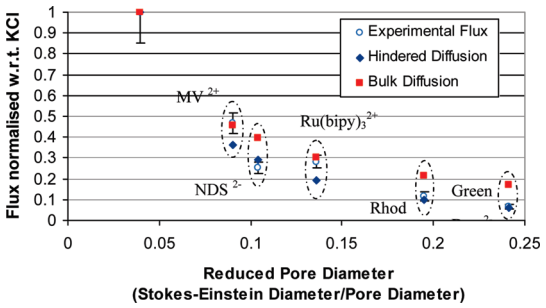

Figure 2. Diffusional flux of the probe molecules normalized to KCl flux. The Stokes–Einstein diameters are calculated from their bulk diffusivities. Reduced pore diameter (λ) varies from 0.04 to 0.24. Data from left to right are KCl, MV^{2+}, NDS^{2-}; Ru-bipy^{2+} rhodamine B; green dye^{2-}. The error bars are at 95% confidence. The bulk diffusion values are from literature precedence, and the hindered diffusion values have been calculated from the Renkin equation based on purely steric interactions between the pore and the permeates.

probe molecules has been calculated from

$$\text{Diffusivity}_{\text{Probe}} = \left(\frac{\text{Flux}_{\text{Probe}}}{\text{Flux}_{\text{KCl}}}\right) \times \text{Diffusivity}_{\text{KCl}} \quad (2)$$

The bulk diffusivity of KCl at 25 °C is assumed to be 1.7×10^{-5} cm^2/s.

For transport in pores of molecular dimensions, there is enhanced interaction between the pore and the molecule. For purely steric interactions between the solute and pore wall, hindered diffusivity, D_h, can be expressed by the Renkin equation as

$$D_h = D_0(1 - \lambda)^2(1 - 2.104\lambda + 2.09\lambda^3 - 0.95\lambda^5) \quad \textbf{(3)}$$

where λ is defined as the reduced pore diameter defined by

$$\lambda = \frac{\text{Stokes} - \text{Einstein Diameter}}{\text{Pore Diameter}} \quad \textbf{(4)}$$

The Stokes–Einstein diameters of the probes were ~6–13 Å, which provided reduced pore diameters up to ~0.24; that is, up to a quarter of the pore diameter was filled with the molecule. The experiments were carried out on the same membrane, with 5 mM of the probe molecule in the feed solution, and the fluxes are normalized to KCl flux of equimolar KCl feed (Figure 2). In general, the fluxes of all the probe molecules lie between the bulk diffusion (red squares) and hindered diffusion (blue diamond) predictions. The hindered diffusion predictions have been calculated from eq 4. Apparently the diffusivity of the positively charged species is closer to bulk diffusion predictions, while the negatively charged species is slower than bulk diffusion predictions (Table 1). This is attributed to the electrostatic interaction of the charged molecules with the charged gatekeeper molecules that are introduced on the membrane surface during water-plasma oxidation process. For the negatively charged species, the permeates are repelled by the negatively charged (carboxylic acid) gatekeeper molecules and are more hindered.[30] The positively charged species are partitioned attractively in the pores, causing the flux to be closer to bulk diffusivity values. It should be possible to obtain a higher electrostatic interaction provided the CNTs are narrower and the electrolyte is dilute enough that it does not screen the charge on the CNT entrances. In a recent work, salt rejection by electrostatic means has been demonstrated in sub-2 nm CNT channels by Fornaseior *et al.* at millimolar salt concentrations.[31] With a view to quantify the effect of the functional molecules on diffusive transport experiments we had estimated the functionalization length of the nanotubes, *i.e.*, the fraction of the length of the tubes that is functionalized, based on Au-nc functionalization experiments on the exterior of the nanotubes.[32] Ongoing research is directed to increase the limited functional density at the CNT entrances by electrochemical grafting techniques to influence the transport properties.[25] Of interest is the possibility to introduce selectivity through chemical interactions, but maintain the extremely fast mass transport properties of the CNTs.

Although we have estimated the diffusion coefficient of the probe molecules with respect to KCl, these monovalent ions (K^+ or Cl^-) are not expected to be adsorbed by CNTs; therefore, KCl is the reference for estimation of the apparent diffusion coefficient. That the ionic diffusion of the molecular species, in this investigation, is close to bulk diffusivity expectations (~10^{-6} cm^2/s) is truly unique for hydrophobic interiors of the CNTs. In contrast, a 200 nm Anopore membrane or a 2 nm Au nanopore membrane made hydrophobic by chemical functionalization would not allow transport of ionic species presumably due to an inability to wet the inner pores.[33] Similarly, adsorption can dominate diffusion of dye molecules in nanoporous silica and has been found to be considerably retarded (~10^{-10} cm^2/s).[34] Theoretical work by Hummer *et al.* suggests that the energy barrier for ions to move from a high dielectric region (solution) to the low dielectric (pore) can be substantially reduced for CNT channels larger than 1 nm, and bulk diffusion would be expected,[35] with our experiments providing evidence for these theoretical estimations. Transport of molecules through CNT channels with minimum mass transport limitations and the presence of charged functional groups at the channel entrance makes the CNT membrane structure an ideal scaffold to mimic biological gatekeeper-like transport.

Gas Transport. Gas transport through mesoporous materials is generally a combination of (i) viscous or Poiseuille flow, (ii) Knudsen diffusion, and (iii) surface diffusion.[36,37] From the perspective of separations, higher flux with lower separation is obtained for viscous flow and lower flux with higher separation for surface diffusion in the order described. Viscous

or Poiseuille permeability, the preferred mechanism in large pores, can be mathematically described by

$$J_P = \frac{\varepsilon_P \mu_{Kn} r^2}{8RT\eta L} P_m \quad (5)$$

where J_P is the Poiseuille permeation (mol m^{-2} s^{-1} Pa^{-1}), μ_P is the reciprocal tortuosity, η is the gas viscosity (N s m^{-2}), L is the thickness (m) of the membrane, and P_m is the mean pressure (Pa), *i.e.*, the mean of the inlet and outlet pressure. Importantly, the Poiseuille permeation scales linearly and inversely with the viscosity. Knudsen diffusion becomes prominent when the mean free path of the diffusing species is larger than the pore diameter, and the Knudsen permeability can be expressed by the following equation:

$$J_{Kn} = \frac{2\varepsilon_p \mu_{Kn} vr}{RTL};\ V = \left(\frac{8RT}{\Pi M}\right)^{0.5} \quad (6)$$

where J_{Kn} is the Knudsen permeation (moles m^{-2} s^{-1} Pa^{-1}), ε_p is the porosity, μ_{Kn} is a shape factor equal to $1/\tau$, r is the pore radius (m), τ is the tortuosity, v is the average molecular velocity (m s^{-1}), L is the layer thickness (m), M is the molecular mass (kg mol^{-1}) of the gas molecule, and T is the absolute temperature (K). Paralleling arguments for the kinetic theory of gases, the characteristics of Knudsen-type transport are inverse scaling with the square root of the molecular weight of the gases. In some cases of porous membranes, a surface-adsorption-based preferential diffusion may lead to highly selective transport.[38,39] A representative equation is

$$J_s = -\rho_{app} D_s \mu_s \frac{dq}{dl} \quad (7)$$

where J_s is the surface diffusion flux component (mol m^{-2} s^{-1}), ρ_{app} is the apparent density (kg m^{-3}), D_s is the surface diffusion coefficient (m^2 s^{-1}), μs is the reciprocal tortuosity, and dq/dl is the surface concentration gradient (mol kg^{-1} m^{-1}).

For most gases at room temperature, the mean free path is significantly larger than the pore diameter of the CNT membrane (~70 Å). For example, air at room temperature will have a mean free path of ~600 Å, which is almost an order of magnitude larger than the pore diameter of the CNT membrane. Hence, one would expect the gas transport through the CNT membranes to be in the Knudsen regime. For transport dominated by viscous flow, the gas permeability should scale linearly with the inverse of viscosity of the gases.[40] Instead the experimental gas permeability[41] scaled with the molecular weight of the gases by an exponent of 0.42, which is close to the predictions of Knudsen diffusion (0.5). Surface-based adsorption-diffusion along the CNT wall may play an important role in the transport of these gases, which might explain the deviation from ideality.[10,42,43]

This observations, *i.e.*, scaling with molecular weight and noncorrelation with viscosity, indicates the absence

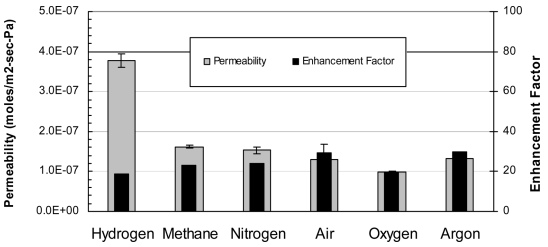

Figure 3. (a) Histogram of observed permeability in (mol/m^2 s Pa) and enhancement factor over Knudsen diffusion for each gas.

of significant viscous transport through the CNT membrane, which would be the case if gas transport was through large cracks or interfacial porosity.[44] The results are also consistent with MD simulations, suggesting insignificant viscous contribution in gas transport through 8.1 nm diameter CNTs.[45]

The expected Knudsen permeability through a pore of 7 nm diameter and 126 μm length (estimated from scanning electron micrographs), $T = 298$ K, tortuosity factor ~1, and porosity ~0.0015 (estimated from KCl diffusion experiments) was calculated from eq 6. The enhancement factor was calculated by the following relation:

$$\text{Enhancement factor} = \text{Experimental permeability}/\text{Calculated Knudsen permeability}$$

Enhancement factors for the gases ranged from 20 to 30 for most gases (Figure 3). It is worth emphasizing that the theory of Knudsen transport is based on the kinetic theory of gases, where momentum transfer is dominated by collisions with the wall. In the case of very smooth surfaces, collisions with the wall will not have any backscattering but will keep all tangential forward momentum upon reflections down the CNT core. For an amorphous carbon-coated (20−30 nm thick) alumina membrane (200 nm pore diameter), gas transport measurements of argon, oxygen, and nitrogen and modeling approaches indicated that approximately 50% of the gas collisions were specular;[46] specular momentum transfer will cause the diffusivities to exceed those predicted from the kinetic theory.[47,48] The observed enhancement factors are in close agreement with other simulations work in graphitic CNTs. For instance, transport diffusivity of Ar (using MD simulations) through a CNT of ~1.6 nm diameter is ~10^{-1} cm^2/s, which is almost 2 orders of magnitude larger than predicted from the Knudsen diffusivity equation (4×10^{-3} cm^2/s).[49] The present observations are also consistent with experimental work on sub-2 nm CNT membranes, where enhancement by 2−3 orders of magnitude was observed.[50] Interestingly, for AAO membranes of comparable pore sizes (~10 nm), gas transport magnitudes were consistent with Knudsen diffusion predictions, whereas a factor of 10 enhancement over Knudsen diffusion was observed for 10 nm track etch polycarbonate membranes.[51] These

TABLE 2. Summary of Pressure-Driven Flow of Liquids through CNT Membranes Using a Syringe Pump Pressure Cell Apparatus[a]

liquid	permeable pore density (# per cm^2)	membrane thickness (μm)	initial permeability (cm^3/cm^2 min bar)	flow velocitynormalized at 1 bar (cm/s)	viscosity (cP)	enhancement factor	slip length (μm)
hexane	3.4×10^9	126	0.44	5.6	0.3	1.09×10^4	9.5
decane	3.4×10^9	126	0.053	0.67	0.9	3.9×10^4	3.4
water (0.7−1 bar)	$1-3.4 \times 10^9$	34−126	0.77(±0.22)	26.1 (±17.2)	1.0	$6\ (\pm 1.6) \times 10^4$	53.3(±14.5)
water (0.001−0.02 bar)	2.4×10^6	81		10.9 (±5.1)	1.0	$4.6\ (\pm 2.1) \times 10^4$	40.4(±18.5)
EtOH	3.4×10^9	126	0.35	4.5	1.1	3.2×10^4	28
IPA	3.4×10^9	126	0.088	1.12	2	1.4×10^4	13

[a] For water flow at ∼0.001−0.02 bar flow is measured by U-tube with positive column height and quantified by $Ru(bipy)_3^{2+}$ dye flow into permeate cell.

observations suggest that the material surface characteristics of the vertically oriented nanoporous materials are critical in obtaining the enhanced diffusivities. The graphitic CNTs with their uniquely large van der Waal distances and atomically smooth interiors are responsible for the enhanced transport rate of gases.

To summarize, the observed permeability of gases scales down with the molecular weight by an exponent ∼0.4, but the diffusivities are ∼2 orders of magnitude larger than Knudsen diffusivity predictions. Thus, a Knudsen-type diffusion transport with highly specular reflection along the CNT walls is the dominating gas transport mechanism. Also the absence of a correlation of transport rates with viscosity is important evidence that the membrane structure consists of molecular channels provided by the inner cores of CNTs.

Liquid Transport. Flow of liquids (J) through porous membranes can be predicted using the Hagen−Poiseuille equation[52] and is given by

$$J = \frac{\varepsilon_p \mu r^2 \Delta P}{8\mu\tau L} \quad (8)$$

where ε_p is the relative porosity, r_0 is the pore radius (3.5 nm for our system), P is the pressure applied, μ is the dynamic viscosity, τ is the tortuosity (1.1), and L is the length of the pore. The basic assumptions of this equation are laminar flow and no-slip at the boundary layer; that is, the velocity of the fluid at the CNT wall is zero.

The implication of the equation for nanoporous materials (small radius) is that the transport rate is limited by the pressure drop across the pores. Modest deviations from the no-slip boundary condition have been achieved for a number of cases including flow through hydrophobic capillaries, thereby providing possibilities to design membranes with small pore size but enhanced liquid transport. However, it has been difficult to make such hydrophobic membranes with dramatically enhanced slip flow, as surface energies would not allow water to enter the transporting channels and require large overpressures to wet the surface. At the microscopic level a conventional hydrophobic surface (with correspondingly large van der Waal distance) can still scatter molecules flowing over the rough interface, thus resulting in near zero average velocity at the interface. In the CNT case once the water is in the tube,[53] it can propagate freely with large slip associated with nearly atomically smooth graphite planes. The effects of both van der Waals distance and atomic smoothness are directly addressed by MD simulations showing the CNT cores as the optimal system.[13] Slip flow can be characterized by slip length, which is an extrapolation of the extra pore radius required to give zero velocity at a hypothetical pore wall (the boundary condition for conventional materials). It indicates the deviation of the liquid flow from the hydrodynamic prediction and denotes the extent of interfacial friction between the liquid and the pore walls. It can be estimated from the equation

$$\frac{V(\varsigma)}{V_{ns}} = 1 + \frac{4\varsigma}{r_0} \quad (9)$$

where $V(\varsigma)$ is the experimentally observed flow velocity (cm/s), V_{ns} is the flow velocity calculated from the Hagen−Poiseuille equation, ς is the slip length, and r_0 is the radius of the nanotube.

The available permeable pore area can be directly measured by diffusion since the diffusion of ions inside CNT pores is close to bulk diffusion, as discussed in the section on ionic transport. Thus by measuring volume flow rate through the CNTs we could directly measure pore flow velocities. In general, the flow velocities were 4−5 orders of magnitude larger than hydrodynamic predictions[20] (Table 2). The trend of flow velocities could not be explained by conventional parameters such as viscosity and hydropbicity. For instance, hexane is less viscous and more hydrophobic than water and should flow faster in a hydrophobic channel than water. However, the hexane flow rate is smaller than water flow through the CNT membrane. MD simulations have shown that water can be transported through CNT channels at extremely high speed by the cooperative movement of a hydrogen-bonded network through the frictionless channels of carbon nanotubes.[54] Most interestingly, the flow velocity of water, *i.e.*, volumetric flow rate through individual nanotubes divided by the pore area, was found to be comparable to those observed in protein channels such as aquaporin and in the MD simulations. However,

TABLE 3. Pressure Flow of Water through CNT Membranes as a Function of Progressive Chemical Functionalization[a]

chemical functionalization	flow velocity normalized at 1 bar (cm/s)	enhancement over Newtonian flow	normalized diffusive flux
as-made (plasma-oxidized)	10.9 (±5.1)	4.6 (±2.1) × 10^4	1
spacer-dye (tip region)	4.7 (±0.7) × 10^{-2}	2 (±0.3) × 10^2	0.93
spacer-dye (core and tip)	<1.26 × 10^{-3}	<5.3	1.03

[a] Flow velocity is measured in the range 0.001—0.2 bar using a U-tube permeation cell with positive column height using a 5 mmol $Ru(bipy)_3^{2+}$ probe molecule and 0.1 M KCl as the screening electrolyte. The enhancement factors are based on calculated no-slip flow (Hagen—Poiseuille) through a pipe with 7 nm inner diameter. Normalized diffusive flux (rightmost column) is the ratio of the observed diffusive flux (without the pressure gradient) after functionalization to the diffusive flux through the as-made (unmodified) CNT membrane and is proportional to permeable pore area.

these experiments do not confirm the presence of ordered water inside the CNT channels. Importantly hexane's flow velocity, though slower than water, was dramatically enhanced, thus indicating that this phenomena does not require H-bond ordering.

The experimental results of liquid flow can be explained by the presence of slip flow conditions at the CNT walls. Theoretically, the existence of micrometer scale slip lengths has been explained by the presence of a gas—liquid interface, which gives rise to a nonzero velocity at the walls.[55,56] The observed slip flow of water is consistent with independent measurements in sub-2 nm CNT channels.[50] The slip length for the liquids was found to correlate qualitatively with the hydrophobicity of the solvent, indicated by the solubility parameter, which is frequently used in the polymer literature to find appropriate solvents.[57] Simply, water, the most hydrophilic of the solvents, has the highest solubility parameter and the maximum slip length of the liquid on the CNT surface. The observed slip lengths are consistent with measured contact angles of polar liquids on CNTs [water (79°) > EtOH (12°) > IPA(8°)].[58] Greater interaction (wetting) of the liquid with the graphite surface leads to a decrease in the slip lengths and decreased transport rates.[59]

In order to test the hypothesis that the enhanced flow observed through the CNT membranes is due to slipping of the liquid at the CNT walls, flow velocities of liquids through the CNT membrane were determined with progressive functionalization of the tips and the core of the CNTs (Table 3). In the diffusion experiments, the liquids in the feed and the permeate cell were maintained at the same level to ensure minimum pressure-driven flux. The pore area was estimated from the diffusive flux measurements with no height

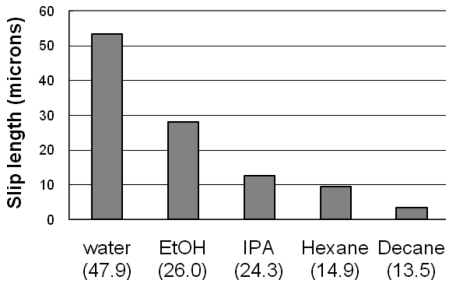

Figure 4. Slip length for various liquids as a function of their solubility parameter (MPa 0.5).

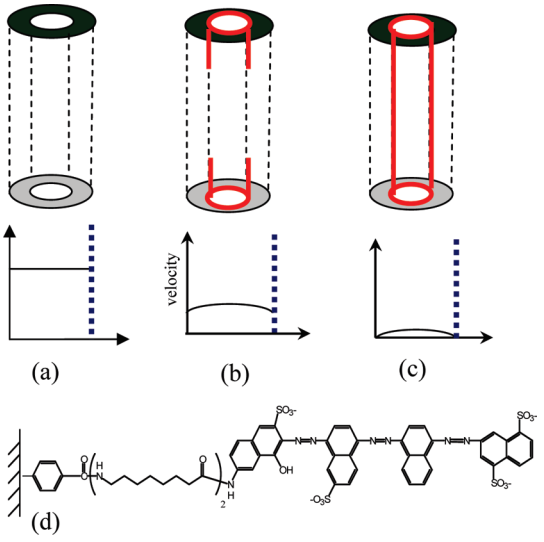

Figure 5. Schematic of sequential functionalization of a CNT membrane corresponding to data shown in Table 3. (a) As-made (plasma-oxidized) membrane without any bulky functional molecules. (b) As-made membrane after functionalization at the tip entrance with a polypeptide linkage and the bulky dye molecule. (c) Interiors of the CNTs grafted by electrochemical diazonium grafting of benzoic acid followed by polypeptide linkage and the dye molecule. (d) Schematic of the functional molecule system utilized in this study.

difference and the assumption of bulk diffusivity of the probe ($Ru(bipy)_3^{2+}$) in the CNT cores. In order to determine the pressure flow velocities, the height of the feed column (5 mmol $Ru(bipy)_3^{2+}$ solution) was deliberately kept ~0.5—20 cm higher than the permeate side. The flow velocity of the water (measured by the concentration of the probe molecule on the permeate side) in the as-made membrane was found to be 8.8(±4.1) cm/s bar (normalized to 1 bar), which is remarkably consistent with the flow velocity of pure water estimated from the syringe pump experiments near 1 bar (~26 cm/s bar). The as-made membrane has carboxyl groups at the CNT tips and was functionalized by a polypeptide spacer and a charged dye molecule containing SO_3^{2-} groups (Figure 5d) using the methods described previously.[26,60] The flow experiment showed that, because of tip functionalization, the velocity the feed solution had decreased 200-fold from 8.8 cm/s to 0.04 (±0.007) cm/s. These experiments

were carried out in the presence of 0.1 M KCl electrolyte in order to screen the electrostatic effects of surface charge,[60] as had been done for the diffusion experiment to measure pore area. To functionalize the entire core of the CNTs, the membrane was grafted electrochemically using diazonium chemistry in static conditions.[60] The membrane was subsequently functionalized with a polypeptide spacer and the anionically charged dye molecule. No detectable pressure-driven transport of the probe molecules was detected in the pressure range of the experiment. The detection limit for this experiment was 5 times the no-slip boundary conditions. In these experiments, the diffusive flux does not change significantly, indicating that the functionalization experiments do not plug the pores, but rather modify the pore-wall and ion/liquid interaction. Most important is that the flow velocity changed over 4 orders of magnitude with the same permeable pore area by changing the surface chemistry, which can only be explained by disruption of the near perfect slip-boundary condition. This experiment directly rules out the possibility of large macroscopic cracks giving erroneously high flow velocities since changing the surface hydrophobicity would have a minimal effect on large crack flow rates. In fact making surfaces more hydrophilic would enhance accessible macroscopic pore areas if that were the primary mechanism. The interpretation of these experiments is shown schematically in Figure 5a–c. These measurements show in a single experiment how the pressure-driven transport through the CNT interior progresses from a slip boundary condition when the interiors are pristine graphitic to a more conventional no-slip boundary condition for CNTs lined with functional molecules. An interesting point is that the carboxyl functionalization from the plasma oxidation process evidently gives the CNT enough hydrophilic nature to promote water entering the CNT core without disrupting rapid flow past the functional groups. With more bulky functional groups the flow is dramatically reduced. The optimal conditions for water flow in terms of extent of hydrophilic carboxylation and whether a monolayer thickness of bulky groups at the CNT entrance also disrupts fast flow are promising areas of future enquiry. However chemical functionality of membrane pores is often required to produce chemical selectivity in membrane-based separations. Thus an important intellectual challenge emerges; functional groups required for chemical selectivity will introduce imperfections on the graphitic nanotubes and dramatically reduce the enhanced flow properties. The key challenges in CNT membrane research lie in identifying strategies for imparting a trade-off between selectivity and the enhanced flow properties by imposing monolayer functionality right at the entrance to the CNT cores or by imparting pumping or acceleration at the region of chemical selectivity.[60,61]

Concluding Remarks. We have experimentally investigated the transport properties through the inner core of CNTs with ~7 nm diameter, *via* macroscopic transport measurements through a membrane structure consisting of substantially dense ($\sim 10^{9-10}$ tubes/cm^2), open-ended, and vertically oriented CNTs in an impermeable polystyrene matrix. Ionic diffusion through the CNT membranes is close to bulk diffusion expectations and electrostatically influenced by a charged carboxyl functionality at the CNT entrance. Gases are transported by a Knudsen-like transport mechanism but are ~15–30-fold faster that Knudsen diffusion predictions due to highly specular reflection at the smooth CNT walls retaining the forward momentum of the gas. Liquid flow through the noninteracting hydrophobic CNT cores is found to be dramatically enhanced, with flow velocities ~1000–10 000 times faster than predictions of liquid transport from conventional no-slip hydrodynamic predictions. The extent of slip decreases with increasing hydrophobicity of the liquid, which is consistent with stronger interactions with the CNT surface reducing the flow enhancement. As direct experimental proof of the mechanism near perfect slip conditions in CNT cores, stepwise hydrophilic functionalization of CNT membranes from as-produced, tip-functionalized, and core-functionalized reduced pressure-driven water flow from 5×10^4 to 2×10^2 to <5 enhancement over conventional Newtonian flow while retaining nearly the same pore area. Carbon nanotube membranes offer an exciting opportunity to mimic natural protein channels due to (1) a mechanism for dramatically enhanced fluid flow through the CNT core, (2) the ability to place gatekeeper chemistry at the entrance to pores, and (3) being electrically conductive to localize electric fields at CNT tips or perform electrochemical transformations. An intellectual puzzle emerges on how to benefit from the fast CNT core velocity while having chemical selectivity that ruins the near perfect slip boundary of pristine CNTs. Nature is able to selectively pump molecules through protein channels, and analogously this can occur with actively pumping selective gatekeepers,[60,61] thereby truly mimicking Nature's remarkable pumps.

METHODS

Ionic Transport Measurements. The probe molecules for ionic transport measurements were methyl viologen dichloride hydrate (98%, Aldrich) [MV^{+2}], tris(2,2′-bipyridyldichlororuthenium(II) hexahydrate [Ru-(bipy)$_3^{2+}$] (Aldrich), 2,6-naphthalenedisulfonic acid, disodium salt (97%, Aldrich) [NDS^{2-}], Fast

Green FCF (99%, Alfa Aesar) [Dye^{2-}], and rhodamine B (Sigma-Aldrich) [Rhod]. The structures of the probe molecules are shown in Table 1. A U-tube diffusion cell for *in situ* measurement by UV−vis (USB-ISS-UV/vis, Ocean Optics Inc.) spectroscopy was used for these experiments. In the setup, a quartz cuvette was converted into the permeate cell and inserted into the UV−vis spectrophotometer to obtain the permeate concentration as a function of time. UV−vis spectra were collected at regular intervals after stirring the permeate solution with a glass pipet. Three different solutions were used for the ionic diffusion studies: (i) a solution of 5 mM in $Ru(bipy)_3^{2+}$ and 5 mM in MV^{2+} for the +ve charged ions, (ii) a solution of 5 mM in NDS^{2-} and Dye $^{2-}$, and (iii) 5 mM of neutral molecule rhodamine B. Nine- to ten-point calibration curves were used for each analyte. Flux rates were obtained by fitting a straight line to the experimentally obtained plot of time *versus* moles of the probe molecules transported plot.

Liquid Transport Measurement. Pressure-driven liquid transport through the CNT membranes was measured in a pressure flow membrane transport setup.[20] Briefly, the membrane was assembled in the flow cell, and a syringe pump provided the required pressure to drive the liquid through the membrane. The weight of the liquid permeating through the membrane was measured in real time on a pan balance interfaced with a laptop computer using Balance Talk SL software from Labtronics.

Water, isopropyl alchohol (IPA), and ethanol (EtOH) were deaerated in a vacuum oven for a period of 12−24 h and allowed to cool under vacuum. For measurements of different liquids on the same membrane, it is dried in air for 12 h and then soaked in the solvent for 1−2 h prior to the experiment. The syringe is then filled with the liquid, and the pipe line is purged with the liquid at 2.5 mL/min flow rate, keeping the valve completely open so that any air in the pipes is driven away. Thereafter, the valve is gradually closed manually to increase pressure inside the flow cell. Once a drop of liquid is seen coming out of the nipple, the data acquisition in the computer is started. Time-dependent pressure data are also collected manually. The zero time for the flow experiments is the time to notice the first drop of liquid coming out of the flow cell. So, there is a systematic error (due to the hold-up volume) in determining the initial permeability. This is significant for liquids such as water, IPA, and EtOH, where the flow rate declines with time. Therefore, an estimate of the hold-up volume was also made. The weight of the bottom plate with a small piece of paraffin was first taken. In place of the CNT membrane, a PAN membrane was used and pressure flow was conducted. The pump was next stopped, and the last drop was allowed to fall out of the nipple. The piece of paraffin was used to close the opening of the nipple. Then the flow cell was disassembled, water poured from the top cell, and water from the bottom cell was dried with Kimwipes and weighed. The difference between the initial and final weights gives the hold-up volume and was found to be ~0.5 cm^3.

Gas Transport Measurement. For gas transport measurements, the same flow cell was used and gas cylinders instead of the syringe pump were used. A small (2 mm) diameter glass capillary, treated with hexyltrimethoxysilane to render it hydrophobic, was attached to the exit of the flow cell. A liquid droplet of ~30 μL was placed inside the capillary, and the volumetric flow of gas permeating was found by timing the movement of the water meniscus between two fixed marks on the glass capillary. A three-step purging protocol was followed to fill the flow cell with gas from the cylinder. (i) The gas line was purged with the gas for 2−3 min. (ii) The control valve was fully opened and the on−off valve was closed so that gas could fill the flow cell. The pressure rose up to ~15 psi. (iii) Then, the valve on the cylinder was closed and the on−off valve was opened to relieve the pressure. Steps (ii) and (iii) were repeated ~10 times to eliminate hold-up gas volume in the flow cell. The flow rate through the glass capillary was calibrated using a syringe pump. The volumetric flow rate through the membrane was measured as a function of the pressure. A linear plot of volumetric flow rate per unit area of the membrane *versus* pressure was obtained, and the slope of the plot was the permeability of the membranes.

KCl Diffusion Experiments for Estimation of Porosity. The pore density and porosity of the membranes was measured using KCl diffusion through the membrane. The feed was 7.5 cm^3 of 669 ppm of KCl (standard solution), while the volume in the permeate side was ~1.5 cm^3. Given that the maximum concentration measured in the permeate is ~25 ppm,the total mass of KCl in the feed solution is about 2 orders of magnitude greater than that in the permeate, thereby eliminating mass depletion effects and ensuring steady-state measurements. Both the feed and the permeate cells were stirred with a magnetic stirrer to enable efficient mixing. The conductivity of the permeate solution was monitored by a conductivity electrode (Microelectrodes Inc.), connected to a conductivity meter (Orion 150 A+ conductivity meter), and the data were collected in a spreadsheet using Balance Talk SL (Labtronics) every 15 min. The conductivity meter was calibrated using a 66.9 ppm standard solution before the start of any experiment. The experimental conductivity data were converted into flux data using an appropriate calibration curve of ppm of KCl *versus* conductivity. The permeable pore area (A_p) can be estimated from the equation

$$A_p = \left(\frac{J \times l}{D \times C}\right)$$

where D is the bulk diffusivity of KCl at 21 °C (~1.7×10^{-5} cm^2/s), C is the concentration of the feed (8.97×10^{-3} M), l is the membrane thickness (from SEM cross sectional pictures), and J is the experimental steady-state flux of KCl (mol/s). The porosity (ε_p) of the membrane and the permeable pore density can be calculated from

$$\varepsilon_p = \left(\frac{A_p}{A_m}\right); \text{ Permeable pore density } (/cm^2) = \frac{\left(\frac{A_p}{A_m}\right)}{\frac{\pi d^2}{4}}$$

where d is the pore diameter (7 nm) and A_m is the membrane area exposed in the diffusion experiment, in this case equal to the area of the O-ring, ~0.3 cm^2. Salt rejection of the CNT membranes was determined by analyzing the permeate solution during a pressure flow of 1.7×10^{-2} (M) KCl; minimal (~4%) salt rejection was observed. Thus, there is not a significant underestimation of A_p from surface charge repulsion.

Acknowledgment. We would like to thank Dali Qian and Rodney Andrews from the Center for Applied Energy, University of Kentucky, for supplying MWCNTs. We also thank Xin Su for the H-TEM image of the MWCNT. Facility support was provided by the Center for Nanoscale Science and Engineering and Electron Microscopy Center at the University of Kentucky. Financial support was from NSF CAREER (0348544)

REFERENCES AND NOTES

1. Murata, K.; Mitsuoka, K.; Hirai, T.; Walz, T.; Agre, P.; Heymann, J. B.; Engel, A.; Fujiyoshi, Y. Structural Determinants of Water Permeation through Aquaporin-1. *Nature* **2000**, *407*, 599–605.
2. Jirage, K. B.; Hulteen, J. C.; Martin, C. R. Nanotubule-Based Molecular-Filtration Membranes. *Science* **1997**, *278*, 655–658.
3. Martin, C. R.; Nishizawa, M.; Jirage, K.; Kang, M. S.; Lee, S. B. Controlling Ion-Transport Selectivity in Gold Nanotubule Membranes. *Adv. Mater.* **2001**, *13*, 1351–1362.
4. Miller, S. A.; Young, V. Y.; Martin, C. R. Electroosmotic Flow in Template-Prepared Carbon Nanotube Membranes. *J. Am. Chem. Soc.* **2001**, *123*, 12335–12342.
5. Steinle, E. D.; Mitchell, D. T.; Wirtz, M.; Lee, S. B.; Young, V. Y.; Martin, C. R. Ion Channel Mimetic Micropore and Nanotube Membrane Sensors. *Anal. Chem.* **2002**, *74*, 2416–2422.
6. Lee, S. B.; Mitchell, D. T.; Trofin, L.; Nevanen, T. K.; Soderlund, H.; Martin, C. R. Antibody-Based Bio-Nanotube Membranes

for Enantiomeric Drug Separations. *Science* **2002**, *296*, 2198–2200.
7. Hummer, G.; Rasaiah, J. C.; Noworyta, J. P. Water Conduction through the Hydrophobic Channel of a Carbon Nanotube. *Nature* **2001**, *414*, 188–190.
8. Sokhan, V. P.; Nicholson, D.; Quirke, N. Fluid Flow in Nanopores: Accurate Boundary Conditions for Carbon Nanotubes. *J. Chem. Phys.* **2002**, *117*, 8531–8539.
9. Ohba, T.; Kanoh, H.; Kaneko, K. Structures and Stability of Water Nanoclusters in Hydrophobic Nanospaces. *Nano Lett.* **2005**, *5*, 227–230.
10. Skoulidas, A. I.; Ackerman, D. M.; Johnson, J. K.; Sholl, D. S. Rapid Transport of Gases in Carbon Nanotubes. *Phys. Rev. Lett.* **2002**, *89*, 185901.
11. Mao, Z. G.; Sinnott, S. B. Separation of Organic Molecular Mixtures in Carbon Nanotubes and Bundles: Molecular Dynamics Simulations. *J. Phys. Chem. B* **2001**, *105*, 6916–6924.
12. Sinnott, S. B.; Mao, Z. A.; Lee, K. H. Computational Studies of Molecular Diffusion through Carbon Nanotube Based Membranes. *Comput. Model. Eng. Sci.* **2002**, *3*, 575–587.
13. Joseph, S.; Aluru, N. R. Why are Carbon Nanotubes Fast Transporters of Water? *Nano Lett* **2008**, *8*, 452–458.
14. Hinds, B. J.; Chopra, N.; Rantell, T.; Andrews, R.; Gavalas, V.; Bachas, L. G. Aligned Multiwalled Carbon Nanotube Membranes. *Science* **2004**, *303*, 62–65.
15. Holt, J. K.; Park, H. G.; Wang, Y. M.; Stadermann, M.; Artyukhin, A. B.; Grigoropoulos, C. P.; Noy, A.; Bakajin, O. Fast Mass Transport through sub-2-Nanometer Carbon Nanotubes. *Science* **2006**, *312*, 1034–1037.
16. Mi, W. L.; Lin, Y. S.; Li, Y. D. Vertically Aligned Carbon Nanotube Membranes on Macroporous Alumina Supports. *J. Membr. Sci.* **2007**, *304*, 1–7.
17. Kim, S.; Jinschek, J. R.; Chen, H.; Sholl, D. S.; Marand, E. Scalable Fabrication of Carbon Nanotube/Polymer Nanocomposite Membranes for High Flux Gas Transport. *Nano Lett.* **2007**, *7*, 2806–2811.
18. Srivastava, A.; Srivastava, O. N.; Talapatra, S.; Vajtai, R.; Ajayan, P. M. Carbon Nanotube Filters. *Nat. Mater.* **2004**, *3*, 610–614.
19. Yu, M.; Funke, H. H.; Falconer, J. L.; Noble, R. D. High Density, Vertically-Aligned Carbon Nanotube Membranes. *Nano Lett.* **2009**, *9*, 225–229.
20. Majumder, M.; Chopra, N.; Andrews, R.; Hinds, B. J. Nanoscale Hydrodynamics—Enhanced Flow in Carbon Nanotubes. *Nature* **2005**, *438*, 44–44.
21. Chiang, I. W.; Brinson, B. E.; Smalley, R. E.; Margrave, J. L.; Hauge, R. H. Purification and Characterization of Single-Wall Carbon Nanotubes. *J. Phys. Chem. B* **2001**, *105*, 1157–1161.
22. Ago, H.; Kugler, T.; Cacialli, F.; Salaneck, W. R.; Shaffer, M. S. P.; Windle, A. H.; Friend, R. H. Work Functions and Surface Functional Groups of Multiwall Carbon Nanotubes. *J. Phys. Chem. B* **1999**, *103*, 8116–8121.
23. Domingo-Garcia, M.; Lopez-Garzon, F. J.; Perez-Mendoza, M. Effect of Some Oxidation Treatments on the Textural Characteristics and Surface Chemical Nature of an Activated Carbon. *J. Colloid Interface Sci.* **2000**, *222*, 233–240.
24. Majumder, M.; Keis, K.; Zhan, X.; Meadows, C.; Cole, J.; Hinds, B. J. Enhanced Electrostatic Modulation of Ionic Diffusion through Carbon Nanotube Membranes by Diazonium Grafting Chemistry. *J. Membr. Sci.* **2008**, *316*, 89–96.
25. Majumder, M.; Keis, K.; Zhan, X.; Meadows, C.; Cole, J.; Hinds, B. J. Enhanced Electrostatic Modulation of Ionic Diffusion through Carbon Nanotube Membranes by Diazonium Grafting Chemistry. *J. Membr. Sci.* **2008**, *316*, 89–96.
26. Majumder, M.; Chopra, N.; Hinds, B. J. Effect of Tip Functionalization on Transport through Vertically Oriented Carbon Nanotube Membranes. *J. Am. Chem. Soc.* **2005**, *127*, 9062–9070.
27. Martin, C. R.; Rubunstein, I.; Bard, A. J. The Heterogenous Rate Constant for the $Ru(bpy)_3^{3+/2+}$ Couple at a Glassy Carbon Electrode in Aqueous Solution. *J. Electroanal. Chem.* **1983**, 151.
28. Armstrong, D. W.; Ward, T. J.; Berthod, A. Miceller Effects on Molecular Diffusion: Theoretical and Chromatographic Considerations. *Anal. Chem.* **1986**, *58*, 579–582.
29. Rani, S. A.; Pitts, B.; Stewart, P. S. Rapid Diffusion of Fluorescent Tracers into *Staphylococcus epidermidis* Biofilms Visualized by Time Lapse Microscopy. *Antimicrob. Agents Chemother.* **2005**, *49*, 728–732.
30. Smith, I.; Frank, G.; Deen, W. M. Electrostatic Effects on the Partitioning of Spherical Colloids between Dilute Bulk Solution and Cylindrical Pores. *J. Colloid Interface Sci.* **1983**, *91*, 571–590.
31. Fornasiero, F.; Park, H. G.; Holt, J. K.; Stadermann, M.; Grigoropoulos, C. P.; Noy, A.; Bakajin, O. Ion Exclusion by sub-2-nm Carbon Nanotube Pores. *Proc. Natl. Acad. Sci.* **2008**, *105*, 17250–17255.
32. Chopra, N.; Majumder, M.; Hinds, B. J. Bifunctional Carbon Nanotubes by Sidewall Protection. *Adv. Funct. Mater.* **2005**, *15*, 858–864.
33. Steinle, E. D.; Mitchell, D. T.; Wirtz, M.; Lee, S. B.; Young, V. Y.; Martin, C. R. Ion Channel Mimetic Micropore and Nanotube Membrane Sensors. *Anal. Chem.* **2002**, *74*, 2416–2422.
34. Fu, Y.; Ye, F.; Sanders, W. G.; Collinson, M. M.; Higgins, D. A. Single Molecule Spectroscopy Studies of Diffusion in Mesoporous Silica Thin Films. *J. Phys. Chem. B* **2006**, *110*, 9164–9170.
35. Peter, C.; Hummer, G., Ion Transport Through Membrane-Spanning Nanopores Studied by Molecular Dynamics Simulations and Continuum Electrostatics Calculations *Biophys. J.* **2005**, *89*, 2222—2234.
36. Cussler, E. L. *Diffusion: Mass Transfer in Fluid Systems*, Second ed.; Cambridge University Press, 2003; pp 176—179.
37. de Lange, R. S. A.; Keizer, K.; Burggraaf, A. J. Analysis and Theory of Gas Transport in Microporous Sol-Gel Derived Ceramic Membranes. *J. Membr. Sci.* **1995**, *104*, 81–100.
38. Rao, M. B.; Sircar, S. Nanoporous Carbon Membranes for Separation of Gas Mixtures by Selective Surface Flow. *J. Membr. Sci.* **1993**, *85*, 253–264.
39. Fuertes, A. B. Adsorption-Selective Carbon Membrane for Gas Separation. *J. Membr. Sci.* **2000**, *177*, 9–16.
40. Yaws, C. L. *Matheson Gas Handbook*, 7th ed.; Mc Graw Hill: New York, 2001.
41. Thorton, A.; Hinds, B. J.; Hill, A.; Majumder, M. Specular Gas Transport in Carbon Nanotube Membranes. *Nano Lett.* **2011**submitted.
42. Bittner, E. W.; Smith, M. R.; Bockrath, B. C. Characterization of the Surfaces of Single-Walled Carbon Nanotubes using Alcohols and Hydrocarbons: a Pulse Adsorption Technique. *Carbon* **2003**, *41*, 1231–1239.
43. Matranga, C.; Bockrath, B.; Chopra, N.; Hinds, B. J.; Andrews, R. Raman Spectroscopic Investigation of Gas Interactions with an Aligned Multiwalled Carbon Nanotube Membrane. *Langmuir* **2006**, *22*, 1235–1240.
44. Roy, S.; Raju, R.; Chuang, H. F.; Cruden, B. A.; Meyyappan, M. Modeling Gas Flow through Microchannels and Nanopores. *J. Appl. Phys.* **2003**, *93*, 4870–4879.
45. Bhatia, S. K.; Chen, H. B.; Sholl, D. S. Comparisons of Diffusive and Viscous Contributions to Transport Coefficients of Light Gases in Single-Walled Carbon Nanotubes. *Molec. Sim.* **2005**, *31*, 643–649.
46. Cooper, S. M.; Cruden, B. A.; Meyyappan, M.; Raju, R.; Roy, S. Gas Transport Characteristics through a Carbon Nanotubule. *Nano Lett.* **2004**, *4*, 377–381.
47. Arya, G.; Chang, H.-C.; Maginn, E. J. Molecular Simulations of Knudsen Wall-slip: Effect of Wall Morphology. *Mol. Simul.* **2003**, *29*, 697.
48. Arya, G.; Chang, H.-C.; Maginn, E. J. Knudsen Diffusivity of a Hard Sphere in a Rough Slit Pore. *Phys. Rev. Lett.* **2003**, *91*, 026102–4.
49. Ackerman, D. M.; Skoulidas, A. I.; Sholl, D. S.; Johnson, J. K. Diffusivities of Ar and Ne in Carbon Nanotubes. *Mol. Simul.* **2003**, *29*, 677–684.
50. Holt, J. K.; Park, H. G.; Wang, Y.; Stadermann, M.; Artyukhin, A. B.; Grigoropoulos, C. P.; Noy, A.; Bakajin, O. Fast Mass Transport Through Sub-2-Nanometer Carbon Nanotubes. *Science* **2006**, *312*, 1034–1037.
51. Roy, S.; Cooper, S. M.; Meyyappan, M.; Cruden, B. A. Single Component Gas Transport through 10 nm

Pores: Experimental Data and Hydrodynamic Prediction. *J. Membr. Sci.* **2005**, *253*, 209–215.
52. Mulder, M. *Basic Principles of Membrane Technology*; Kluwer Academic Publishers: Dordrecht, The Netherlands, 1997.
53. Naguib, N.; Ye, H. H.; Gogotsi, Y.; Yazicioglu, A. G.; Megaridis, C. M.; Yoshimura, M. Observation of Water Confined in Nanometer Channels of Closed Carbon Nanotubes. *Nano Lett.* **2004**, *4*, 2237–2243.
54. Hummer, G.; Rasaiah, J. C.; Noworyta, J. P. Water Conduction through the Hydrophobic Channel of a Carbon Nanotube. *Nature* **2001**, *414*, 188–190.
55. Lauga, E.; Brenner, M. P. Dynamic Mechanisms for Apparent Slip on Hydrophobic Surfaces. *Phys. Rev. E: Stat., Nonlinear, Soft Matter Phys.* **2004**, *70*, 026311–7.
56. de Gennes, P. G. On Fluid/Wall Slippage. *Langmuir* **2002**, *18*, 3413–3414.
57. Grulke, J. B. E. H. I. E. A. *Polymer Handbook*, fourth ed.; John Wiley and Sons, Inc.: New York, 1999; pp VII/675−711.
58. Mattia, D.; Bau, H. H.; Gogotsi, Y. Wetting of CVD Carbon Films by Polar and Nonpolar Liquids and Implications for Carbon Nanopipes. *Langmuir* **2006**, *22*, 1789–1794.
59. Zhu, Y.; Granick, S. Rate-Dependent Slip of Newtonian Liquid at Smooth Surfaces. *Phys. Rev. Lett.* **2001**, *87*), 096105.
60. Majumder, M.; Zhan, X.; Andrews, R.; Hinds, B. J. Voltage Gated Carbon Nanotube Membranes. *Langmuir* **2007**, *23*, 8624–8631.
61. Wu, J.; Paudel, K. S.; Strasinger, C.; Hammell, D.; Stinchcomb, A. L.; Hinds, B. J. Programmable Transdermal Drug Delivery of Nicotine Using Carbon Nanotube Membranes. *Proc. Natl. Acad. Sci.* **2010**, *107*, 11698–11702.